

L^3 F-TOUCH: A Light-weight, Low-cost, and WireLess GelSight with Extended Force Sensing

Wanlin Li^{1*}, Meng Wang^{1*}, Jiarui Li^{1,2}, Yao Su¹, Devesh K. Jha³, Xinyuan Qian⁴, Kaspar Althoefer⁵ and Hangxin Liu¹

Abstract—By reconstructing the deformation of its soft elastomer through imaging techniques, the GelSight sensor can estimate contact geometry and force in a super high spatial resolution. Despite its increasing popularity, this tactile sensing mechanism yields poor force measurements when the elastomer deforms uniformly or when the deformation saturates. This paper presents L^3 F-TOUCH sensor, an enhanced version of the classic GelSight sensor, to acquire a much better three-axis force sensing capability while being Light-weight, Low-cost and wireLess for the ease of replication and deployment. Specifically, L^3 F-TOUCH consists of (i) an elastomer structure that follows the typical GelSight sensor design to sense fine-grained contact geometry, and (ii) a mechanically simple suspension structure comprised of stiff parallel springs, which enables three-dimensional elastic displacements of the elastomer structure upon contacts. To effectively track the displacement and correlate that to three-axis contact force, a miniature tracking system is developed using the camera in the elastomer structure to track a marker printed on the suspension base through a mirror. In a set of evaluations and experiments, the proposed L^3 F-TOUCH demonstrates a significantly improved force sensing capability compared to other GelSight designs while being much lighter and cost-effective compared to commercial three-axis force sensors. The wireless data transmission feature also enables broader applications of akin vision-based tactile sensors.

Index Terms—GelSight sensor, vision-based tactile sensor

I. INTRODUCTION

THE ability to sense contact forces is an essential feature of human tactile system. We rely heavily on force and tactile sensing to perform various grasping and manipulation tasks [1, 2]. It has been the long-standing goal in robotics to enable robots with human-level dexterity during manipulation and grasping. Thus, it is pivotal that robots should also have a reliable sense of touch and contact forces. In recent years, vision-based tactile sensors, *e.g.* GelSight sensor [3] and its variants [4–7], have emerged as an effective means to achieve this goal. The idea behind GelSight sensing technique is

* Wanlin Li and Meng Wang contributed equally to this work.

¹ National Key Laboratory of General Artificial Intelligence, Beijing Institute for General Artificial Intelligence (BIGAI), Beijing 100080, China. Emails:{liwanlin, wangmeng, lijiarui, suyao, liuhx}@bigai.ai.

² College of Engineering, Peking University, Beijing 100871, China.

³ Mitsubishi Electric Research Labs (MERL), Cambridge, MA 02139, USA. Email: jha@merl.com

⁴ Department of Computer and Communication Engineering, University of Science and Technology Beijing, Beijing, 100083, China. Email: qianxy@ustb.edu.cn

⁵ Centre for Advanced Robotics @ Queen Mary (ARQ), Queen Mary University of London, UK. Email: k.althoefer@qmul.ac.uk

The design is open-sourced at: <https://github.com/wangmeng13thu/L3-F-TOUCH>.

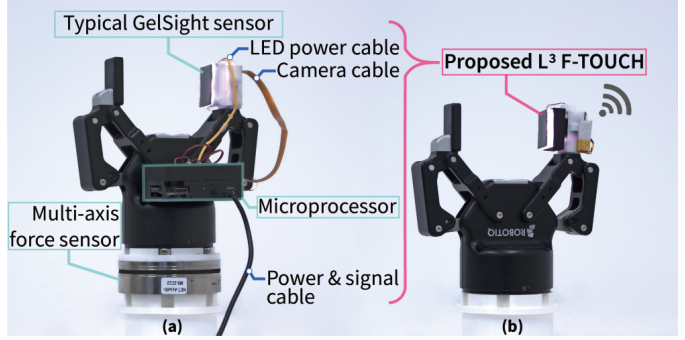


Fig. 1: **Tactile and force sensing in robot manipulation.** (a) A typical integration of a GelSight sensor for fine-grained tactile sensing and a multi-axis force sensor mounted on the manipulator’s wrist for better force sensing. (b) To alleviate complex cabling issues and undesired bulkiness, the proposed L^3 F-TOUCH retains the tactile sensing capability of a GelSight sensor and extends its range of three-axis force sensing. A wireless data transmission module is further integrated for easy deployment and broader applications.

to reconstruct the deformation of its soft elastomer caused by external objects using images captured by an embedded camera. In addition to the contact geometry, normal and shear forces can be further inferred from the deformation as well. Compared with commercial force sensors like transducers and strain gauges [8] or high-end tactile sensors like BioTac [9] and e-skins [10–12], GelSight sensors have the advantages of being low-cost and easy-to-replicate, while achieving a pixel-level spatial resolution in measurements. As a result, they have expanded robots’ capabilities in grasping greatly, such as handling fragile object [13], manipulating deformable items [14], classifying materials [15], estimating object’s hardness [16].

However, the force sensing mechanism of GelSight sensors falls short in two aspects: (i) it cannot measure forces when the elastomer deforms uniformly, *i.e.* when touching a large flat surface, the reconstruction of elastomer’s surface normal will be prevented because the brightness changes cannot be effectively picked up by the camera; (ii) the range of its force sensing is limited by the thickness of its elastomer—it would saturate when the elastomer cannot deform any more—especially when the latest GelSight designs are becoming slimmer with thin elastomer [17–19].

To succeed in more forceful grasping and manipulation tasks [19–21], a multi-axis force sensor is usually mounted on the wrist of a robot’s arm to complement the GelSight sensor installed at gripper’s fingertip; a typical setup is shown in Fig. 1a. This setup is not ideal in that it occupies more payload of the robot arm, introduces errors when synchro-

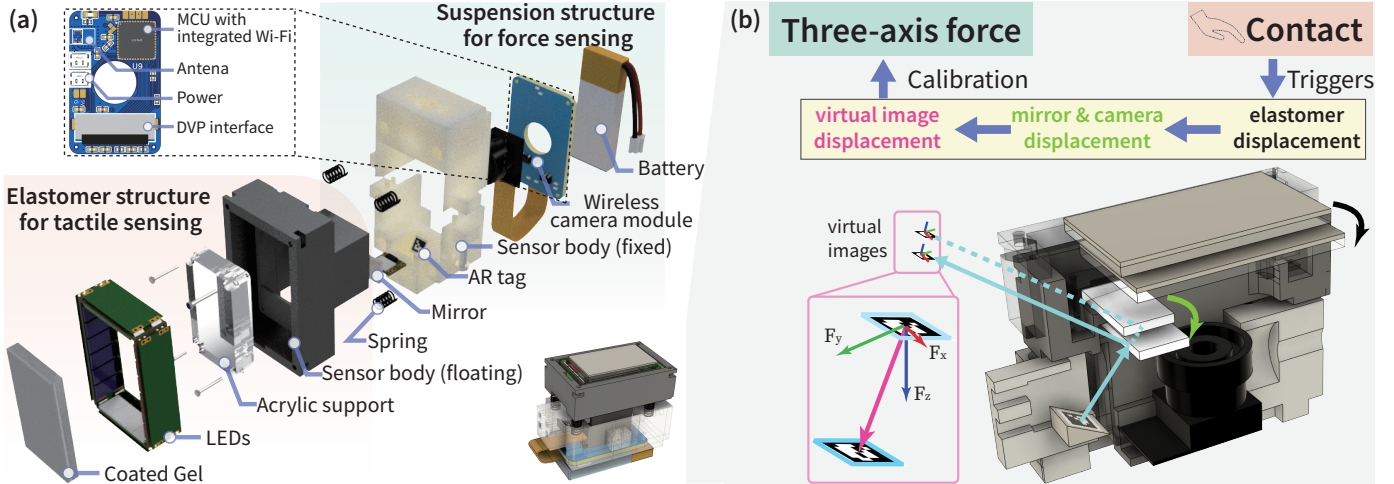


Fig. 2: L³ F-TOUCH sensor design and its force sensing principle. (a) The sensor consists of two parts: The elastomer structure attains a super high spatial resolution in sensing contact geometry. Using stiff springs, the suspension structure allows the elastomer to float and displace upon contact. A PCB is designed to remotely transmit camera images to a workstation and to power the sensor with a battery. (b) Under contact, the AR Tag fixed in the suspension would be projected to a different image coordinate in the camera's view due to the displacement of the mirror installed underneath the elastomer. Such displacements can be transformed into three-axis contact forces through calibration.

nizing and calibrating the two sensors, and measures force far away from the actual contact point. These deficiencies call for a new sensor design that can combine a sufficient range of force sensing and fine-grained contact geometry sensing. In this paper, we present L³ F-TOUCH (Force and Tactile Optically Unified Coherent Haptics), see Fig. 1b, a new design that integrates an elastomer structure equipped with the GelSight sensing technique to a mechanically simple suspension structure comprised of stiff parallel springs. Upon external contact, the elastomer structure will undergo three-dimensional elastic displacement, which is corresponded to three-axis force via calibration. Therefore, L³ F-TOUCH not only measures contact geometry through its elastomer as a GelSight, but also acquires a much larger range of three-axis force sensing.

To capture the displacement of the suspended elastomer structure, we design an optical-based tracking mechanism by leveraging the camera used to capture the elastomer's deformation, without introducing a new sensory component. More specifically, a mirror that would move along with the elastomer structure is installed to reflect and project an AR Tag printed on the fixed suspension base to the camera. The size and pose of the AR Tag detected in the mirror will deviate from its original configuration under different contacts, which becomes a simple yet effective indicator of the relative displacement between the elastomer and the suspension structure. A calibration protocol is subsequently developed to transform the displacements to a three-axis contact force, achieving a significantly larger range compared with that of a GelSight sensor. Together with some new customization, the L³ F-TOUCH reveals the following three advantageous characteristics:

- 1) **Light-weight.** The suspension structure significantly extends traditional GelSight sensors' range of force sensing while remaining small and light enough to be installed at the fingertips as other compact tactile sensors do.

- 2) **Low-cost.** The force sensing mechanism of L³ F-TOUCH does not require new sensors or complex structures, thus not adding much cost in fabrication compared with that of a GelSight sensor. It is also significantly more economical than many commercial three-axis force sensors.
- 3) **WireLess.** The entire sensor can run on battery and we further design a wireless camera module to stream images to a remote workstation in real time. Such a convenient design affords new opportunities for deploying image-based tactile sensors on mobile platforms.

A. Related Work

Utilizing computer vision techniques, Vision-based Tactile Sensor (VBTS) (*e.g.* GelSight [13, 22]) can reconstruct contact surface in a pixel-level spatial resolution and estimate force distribution with a layer of printed marker arrays [23]. To be more compatible with robotic grippers, later modifications on GelSight sensor seek to reduce its overall dimension by utilizing a mirror to bend the camera's view angle (*e.g.* Gelslim [17], GelSight wedge [19]), introducing a delicately small silicone layer (*e.g.* DIGIT [18], DenseTact [6]), or incorporating tactile fingertip sensor [24]. While being more compact, the range and accuracy of a GelSight sensor's force sensing are strictly limited by the deformation range of its elastomer layer—the force reading would saturate when the elastomer reaches its maximal deformation. Thus, an additional instrument such as the force/torque sensor is required when applying GelSight sensors in delicate or forceful grasping scenarios.

On the other hand, Li *et al.* developed the F-TOUCH sensor that utilized a spring-mechanism structure suspending the Gel to enhance VBTS's force sensing capability [4]. Ouyang *et al.* introduced a fiducial-based multi-axis force/torque sensor [25]. Nozu *et al.* used two layers of transparent elastomer sandwiching an acrylic board to improve the accuracy in three-axis force sensing [26]. Although these designs better offset the

limitation of GelSight sensor's force sensing capability, they still introduced a more complex structure with extra weight and fabrication cost. Through the integration of a simple suspension structure, the presented L³ F-TOUCH acquires a much larger force sensing while remaining light and compact by not using extra sensory components. A wireless camera module is further added to allow easy deployment of L³ F-TOUCH at the gripper's fingertips and even at drones.

B. Overview

The remainder of this paper is organized as follows. Section II presents the hardware design, the force sensing principle, and the fabrication details of our L³ F-TOUCH sensor. Section III and Section IV describes the force calibration method and the sensor's evaluation results. A series of experiments in Section V further demonstrate the capability and advantage of L³ F-TOUCH sensor. Finally, we conclude the paper with a discussion in Section VI.

II. SENSOR DESIGN AND FABRICATION

The proposed L³ F-TOUCH sensor aims to enhance the GelSight sensor's force sensing while inheriting its advantages of being (i) compact and light-weight for installation at the jaw gripper's fingertips, and (ii) cost-effective, easy-to-replicate, and easy-to-deploy. To achieve these goals, L³ F-TOUCH sensor adopts the classic GelSight sensor design to fabricate an elastomer structure for sensing contact geometry and introduces a spring suspension structure to enable the elastomer's floating motions under contact. The motions are tracked by a marker-based visual detection scheme and transformed into a three-axis contact force. Thus, L³ F-TOUCH sensor can be made in a small form factor and attains a wider range of applications. Below we first briefly describe the major components of L³ F-TOUCH, followed by its detailed fabrication process.

A. Elastomer Structure

Following the design principle of GelSight sensor, the elastomer structure of L³ F-TOUCH consists of five major components, as shown in the left part of Fig. 2a. The slim cuboid elastomer is made from transparent gel with a marker array and opaque matte reflective coating printed on the top. A clear acrylic board is placed under the elastomer for support, around which an internal multi-color LEDs light source is attached to provide uniform illumination. The sensor body is designed and 3D printed to enclose the above components while holding a mirror and a micro camera with a wide-angle lens inside. Of note, although the sensor body is suspended to enable floating motions when contact occurs, the camera view to the Gel remains fixed during motion.

B. Suspension Structure

To extend the force sensing capability, a mechanically simple but reliable suspension structure comprised of stiff parallel springs is proposed. As shown in the right part of Fig. 2a, the fixed sensor body includes a "4 × 4_50" ArUco tag with a size of 3 mm affixed to a 40° tilted slope, a PCB

to acquire camera images and transmits them wirelessly to the workstation, and a portable battery that powers the entire sensor. Four parallel springs are installed in the fixed sensor body to support the floating elastomer structure.

With this suspension structure, the contact force exerted on the sensor not only deforms the Gel, but also leads to multi-axis floating motions of the elastomer structure due to the elastic compression of the parallel springs. The camera inside the elastomer structure would observe both the tactile imprint for reconstructing contact geometry and the ArUco tag projected pose, which is different as the mirror moves, for measuring contact force; Fig. 2b further illustrates this idea. Note that the tactile imprint and the tag's pose are decoupled, which simplifies the sensor's calibration process.

C. Fabrication Details

Wireless Camera Module: We manufactured a PCB (see Fig. 2a) to make the L³ F-TOUCH more compact and easier to deploy. It integrates a power supply circuit for all electronic components of the sensor, a Digital Video Port (DVP) that connects to the camera, and an ESP32-PICO-V3-02 microcontroller unit (MCU) with a 2.4G ceramic antenna to stream the captured images to a remote workstation. An RTSP server is running in the MCU to stream images in MJPEG format with a resolution of 640 × 480 at a frame rate of 26 FPS. Section IV provides a further study on the balance between sampling frequency, latency, and image resolution. As a result, the dimension of the L³ F-TOUCH is minimized to 40 × 25 × 35 mm (L × W × H) with a total weight of 25 g. The entire sensor runs on a 3.7V LiPo battery.

Illumination: We used surface-mounted LED in four colors (red, green, blue and white) to illuminate the coated gel and a white LED to light up the tag. In order to optimize the image quality captured by the camera, we chose LUXEON 2835 Color Line SMD LED which is not only small in size (3.5 × 2.8 × 0.7 mm) but also provides a full-color palette for a wide spectrum range. The spectrum response of both the camera and the LEDs were compared for the RGB color selection, the gray filters (VViViD Air-Tint Dark Air-Release Vinyl Wrap Film) and diffusers (3M Diffuser 3635-70) were stuck to the side of the acrylic sheet to effectively improve the contrast and uniformity of tactile frames [19].

Coated Gel: As the suspension structure of the L³ F-TOUCH enables large-range force measurement, we can reduce the thickness and hardness of the coated Gel. We used Smooth-On Solaris part A&B (Shore A 15) as the clear base

TABLE I: The bill of materials (BOM) of L³ F-TOUCH sensor.

	Part	Description	Qty	Cost
Elastomer	Camera	OV2640 with 160° lens	1	\$3
	LEDs	RGBWhite SMD LEDs	20	\$5
	Mirror	5 × 10 × 1 mm	1	\$1
	Gel	Base + marker + coating	1	\$5
Suspension	3D printed housing	Elastomer structure body	1	\$3
	Spring	0.4 × 3 × 5 mm	4	\$1
	Electronic components	PCB, MCU, etc.	1	\$6
	Battery	400mAh 1-cell LiPo	1	\$2
	3D printed housing	Suspension structure body	2	\$3
	Misc items	Glue, printed Aruco marker	2	\$2
Total costs				\$31

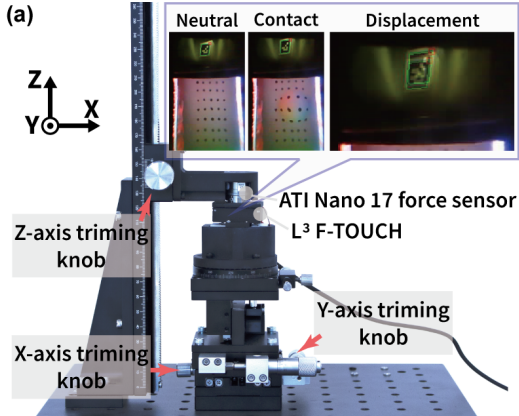


Fig. 3: **The force calibration setup.** (a) A L³ F-TOUCH sensor is installed on an XYZ 3-Axis Linear Stage Trimming Platform. A commercial ATI force/torque sensor is used to collect ground-truth force data. Initially, the ATI sensor is trimmed down to just contact the elastomer structure, which serves as the reference point. (b) By trimming the sensor in 5 directions, the correspondence between the three-axis force and the three-axis displacement of the virtual AR Tag is acquired.

with a thickness of 1.5 mm. Smooth-On Slacker was then added as the silicone thinner. The weighted ratio of each ingredient is 1 : 1 : 3 (part A: part B: thinner). Finally, a 5 × 7 black marker array is painted with Smooth-On Silc Pig black colorant on the top surface. For the coating layer, we used mill-resistant matte oil to protect the surface of the silicone rubber, and mixed it with spherical aluminum powder to produce a Lambertian surface. We airbrushed the diluted mixture on the surface of the base to form a reflective and protective coating layer.

Total Cost: Table I provides the bill of materials of the L³ F-TOUCH and the cost for each major component. Compared to commercial micro multi-axis F/T sensors that cost thousands of dollars and require wired and bulky peripherals, the total material cost of a L³ F-TOUCH can be as low as \$30, and the majority of the components are off-the-shelf. In addition, we open source the entire hardware design and processing software of the L³ F-TOUCH to further promote its applications. Therefore, L³ F-TOUCH is an inexpensive sensor that can be manufactured easily to provide a sufficient tactile and forcing sensing capability.

III. SENSOR CALIBRATION

This section describes the calibration of the L³ F-TOUCH sensor from two aspects: multi-axis force calibration and tactile imprint calibration. Since these two modalities are decoupled, each calibration process can be operated individually. Besides, due to the distortion from the wide-lens camera, we first apply a standard camera calibration to rectify the captured frame [27].

A. Force Calibration

In our design, the external force $\mathbf{F} = \{F_x, F_y, F_z\}$ applied to the sensor eventually causes the displacement of the mirrored tag $\mathbf{D} = \{D_x, D_y, D_z\}$ in the camera's image coordinate; see Fig. 2b. Thus, the force calibration is to establish a transformation between \mathbf{F} and \mathbf{D} . Here we simplified the transformation in a linear term:

$$\begin{bmatrix} K_{3 \times 3} \\ Bias \end{bmatrix} \cdot \begin{bmatrix} D_x \\ D_y \\ D_z \end{bmatrix} + \begin{bmatrix} F_x \\ F_y \\ F_z \end{bmatrix}, \quad (1)$$

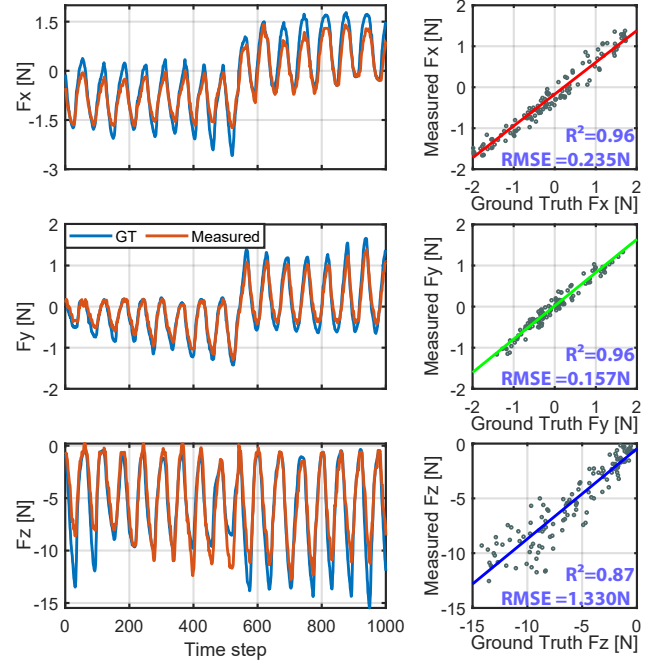


Fig. 4: **Force calibration results.** *Left:* The comparison between the force measured by our L³ F-TOUCH sensor and by the ATI Nano 17 shows a good correspondence. *Right:* In x and y-axis, the L³ F-TOUCH's force measurement achieves a good accuracy and high linearity, indicated by the low RMSE and high R^2 , respectively. The result in z-axis is not as ideal, but is still good given its much larger range.

where $K_{3 \times 3}$ maps the coupled effects between the displacement and the force. Given the camera's calibration parameters (intrinsic matrix, radial, and tangential distortions) and the marker's geometric dimension, the mirrored marker's displacement \mathbf{D} can be efficiently measured by solving the Perspective-n-Point (PnP) problem.

The calibration setup is shown in Fig. 3a. We used an XYZ 3-Axis linear stage trimming platform to control the displacement of the floating elastomer structure, and the corresponding force reading that serves as the ground-truth is measured by an ATI Nano17 6-axis F/T sensor. The ATI sensor placed on the

Z stage is trimmed down to initiate contact with the elastomer structure, which is referred to as the *Rest* condition, *i.e.* 0 mm in Z. Then, we collected a dataset of tag displacements under five controlled conditions: trimming ± 1.5 mm in X-axis, ± 1.5 mm in Y-axis, and -2 mm in Z. In each condition, the trim positions other than that in the axis-of-interest are set to 0. The correlations between the resulting displacement of the mirrored AR Tag D_x, D_y, D_z and the corresponding forces F_x, F_y, F_z are shown in Fig. 3b. Based on this dataset, we solve for Eq. (1) by the least squares method, and Fig. 4 shows the calibrated result.

B. Tactile Mode Calibration

The elastomer structure of the L³ F-TOUCH is by itself a GelSight sensor. To leverage its advantage of sensing contact geometry, we also perform a tactile calibration for L³ F-TOUCH following the established procedure for that of a GelSight. Below we briefly describe the procedure and refer interested readers to [3] for details.

Reconstructing contact geometry: The principle of the GelSight approach is to measure deformation upon contact by mapping the *RGB* color intensity of the frame to its corresponding horizontal and vertical surface gradients g_x, g_y and integrating them at each pixel to obtain the depth. Typically, a look-up table that maps *RGB* to g_x, g_y is needed [22]. To build this look-up table, we collect tactile frames with a known-size metallic sphere pressing upon the gel. In each frame, the sphere casts a circular contact whose center c_x, c_y and radius r are measured to calculate the gradient g_x, g_y based on the contact volume of the sphere; the gradients correspond to pixel intensity within the contact region.

Measuring contact force: Marker arrays can be painted within the silicone coating layer for distributed force sensing. One common way [19] is to directly use the marker's displacement in the tactile imprint to represent the shear force distribution, as they can be approximated as positively correlated. Another method is based on elastostatic theory to establish a global relationship between the field of marker motions and the field of applied forces using inverse FEM (iFEM) [17]. However, it is hard to precisely describe the model and accurately conduct the calibration procedure since the deformation of the elastomer is nonlinear. Notably, L³ F-TOUCH alleviates this limitation by using the suspension structure to sense force; we use the elastomer structure to measure contact force only for comparison studies that demonstrate the L³ F-TOUCH's advantage in force sensing.

IV. SENSOR EVALUATION

We characterize the force sensing capability of L³ F-TOUCH sensor, *i.e.* the efficacy of the suspension structure, from the following six aspects. Due to the intensive study conducted on GelSight sensors in the literature [3], we do not provide a further evaluation of the elastomer structure.

Linearity shows how the sensor output is proportional to the input. Based on the calibration data collected from Fig. 3 and the regression model obtained from Eq. (1), the right part of Fig. 4 shows the linearity result of L³ F-TOUCH sensor, where the root mean square error (*RMSE*)

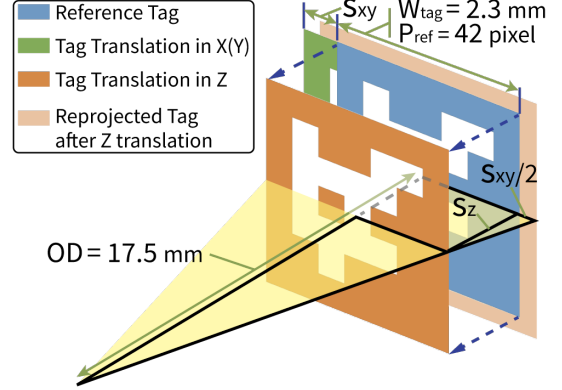


Fig. 5: **Schematic view of the tag translation and sensitivity.** The optical model is simplified as a symmetric diagram around the optical axis. The green tag indicates an X(Y) translation s_{xy} which results in a 1 pixel translation of the tag image. The red tag indicates a Z translation s_z which results in 1 pixel width change of the tag image.

is of 0.2346 N, 0.1573 N, and 1.33 N and R-square is of 0.96, 0.96 and 0.87 in F_x, F_y and F_z . The fitting in z axis is less ideal than that in xy plane due to the sensor sensitivity investigated below.

Range is the maximum and minimum values the sensor can measure. The maximum output is determined by the reliability of the transformation between the displacement of the mirrored tag and the force. From the calibration result observed in Fig. 4, the range is determined as ± 2 N in xy plane and 12 N in z direction; within the range, the sensor maintains high linearity.

Sensitivity indicates the smallest change in the signal that affects the sensor's output. Based on the optical model of L³ F-TOUCH conceptualized in Fig. 5, we compute the minimal detectable change of the AR Tag and correspond that to the output force according to the calibration matrix. Knowing the default discernible resolution of the tag is $R = 1$ pixel [28], the tag's actual width to the camera $W_{tag} = 3.0$ mm \times $\cos 40^\circ = 2.3$ mm as it is printed with a 40° inclination, and the tag occupies $P_{ref} = 42$ pixel in the image plane under the rest condition, we can calculate the minimum detectable displacement of the tag in x and y direction from the image:

$$s_{xy} = \frac{W_{tag}}{P_{ref}} R = \frac{2.3}{42} \times 1 = 0.055 \text{ mm/pixel}. \quad (2)$$

Similarly, given the object distance measured as $OD = 17.5$ mm, the tag's minimal detectable displacement in z direction is

$$s_z = \frac{OD}{(W_{tag} + s_{xy})/2} \frac{s_{xy}}{2} = 0.409 \text{ mm/pixel}. \quad (3)$$

Given the calibration matrix $K_{3 \times 3}$, we can obtain the corresponding sensitivity of three-axis forces S_x, S_y , and S_z as follows:

$$\begin{bmatrix} S_x \\ S_y \\ S_z \end{bmatrix} = \begin{bmatrix} & K_{3 \times 3} & \end{bmatrix} \cdot \begin{bmatrix} s_{xy} \\ s_{xy} \\ s_z \end{bmatrix} = \begin{bmatrix} 0.070 \\ 0.067 \\ 0.324 \end{bmatrix} \text{ N/pixel}. \quad (4)$$

Repeatability measures how well the sensor can produce the same output under the same input condition. Using the calibration setting in Fig. 3a, we control the Z-axis trimming knob to repeat the same loading and unloading process for

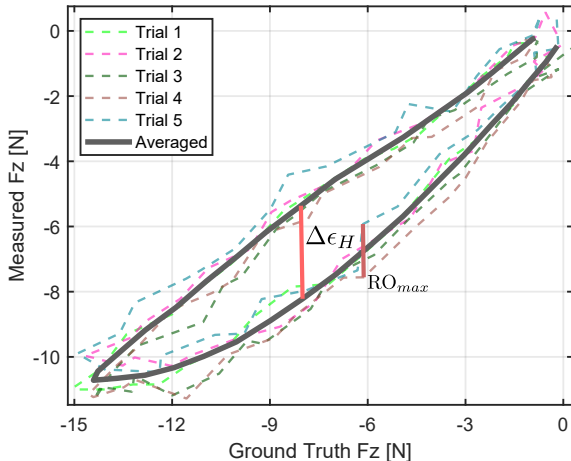


Fig. 6: **Repeatability and hysteresis properties of the L³ F-TOUCH sensor.** Five trials of identical loading and unloading processes were conducted and shown by the dashed lines. They were averaged and plotted as the black curve with smoothing to better reflect the sensor's hysteresis.

5 trials. The comparison between measured and ground truth forces are plotted as the dashed lines in Fig. 6. Then, the repeatability of L³ F-TOUCH is calculated as:

$$\text{Repeatability}(z) = \frac{\Delta RO_{max}}{\varepsilon_{SO}} \times 100\% = 11\%, \quad (5)$$

where $\varepsilon_{SO} = 12 \text{ N}$ is the maximal F_z applied in this study and $\Delta RO_{max} = 1.63 \text{ N}$ is the maximal difference at the same time step across all trials. Note that here we are more interested in the force in the normal direction, *i.e.* F_z due to its central role in grasping; the repeatability of F_x and F_y be investigated following the same procedure.

Hysteresis reflects the difference in the sensor reading during loading and unloading. The solid black curve in Fig. 6 is the average of the 5 trials measured above with a moving average smoothing. Based on this curve, the maximum difference between two processes $\Delta\epsilon_H$ is observed as 2.86 N, and the hysteresis is calculated as

$$\text{Hysteresis}(z) = \frac{\Delta\epsilon_H}{\varepsilon_{SO}} \times 100\% = 25\%. \quad (6)$$

As can be seen that the output values under loading are larger than the unloading process, the main reason could be attributed to the viscoelasticity effect in the connection of compression springs during sensor manufacturing.

Bandwidth and latency analysis is critical for L³ F-TOUCH as it relies on wireless communication to stream camera images. We tested 6 most commonly used display resolutions listed in Table II for L³ F-TOUCH's image acquisition and streaming, and compared them with a wired version of GelSight sensor with the same hardware specification. The traditional GelSight sensor can maintain a stable 30 FPS across all settings. Still, the proposed L³ F-TOUCH has a 26 FPS for VGA (640×480), and it can achieve a higher frame rate by lowering the resolution. Thus, we adopted VGA as the default display resolution, which is a balance between preserving more information from the image and having only a marginally lower frame rate. On the other hand, sensor latency is not

TABLE II: **Frame rate and latency comparison between L³ F-TOUCH and wired GelSight sensor.** Under six different display resolutions, each sensor would run for three 5-min trials. The frame rate was computed based on the number of images received in the workstation within the time interval. The latency would fluctuate over time and was manually monitored; only a range was provided.

Resolution	GelSight		L ³ F-TOUCH	
	frame rate [FPS]	latency [ms]	frame rate [FPS]	latency [ms]
QQVGA(160 × 120)	30		28	
HQVGA(240 × 176)	30		27	
QVGA(320 × 240)	30	~100	27	
HVGA(480 × 320)	30	~100	26	
VGA(640 × 480)	30	150	26	~300
SVGA(800 × 600)	30	150	20	

significantly affected by resolutions. But wireless communication introduced a higher latency in streaming due to network condition, transferring protocol, and decoding configurations, which can be further optimized to a level comparable to that of wired GelSight [29]. Overall, the wireless feature of L³ F-TOUCH does not degrade the sensor's data acquisition compared with that of classic GelSight sensor [3], but it enables a much easier setup under different scenarios.

V. EXPERIMENT AND APPLICATION

This section presents three unique advantages of the proposed L³ F-TOUCH sensor. First, we demonstrated the force sensing range of the L³ F-TOUCH is significantly enlarged by the suspension structure. Second, we validated the necessity of integrating both tactile and force sensing in L³ F-TOUCH when grasping fragile objects or large objects with a flat surface. Finally, we showcased a novel application of L³ F-TOUCH on a drone due to its wireless feature.

A. Extended Force Sensing

In this task, we used the trimming platform in Fig. 3 to press a 4 mm diameter sphere against the sensor as an indenter in the vertical direction and compared the force measurements obtained from the L³ F-TOUCH and the elastomer structure

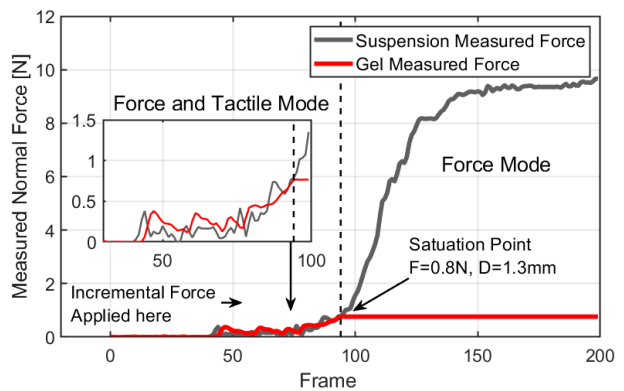


Fig. 7: **The force measurement obtained from the suspension structure and the elastomer of the L³ F-TOUCH.** The force sensing of the elastomer was saturated at 0.8 N with the maximal deformation of 1.3 mm. Incorporating the suspension underneath the elastomer resulted in a 10 times larger force sensing range.

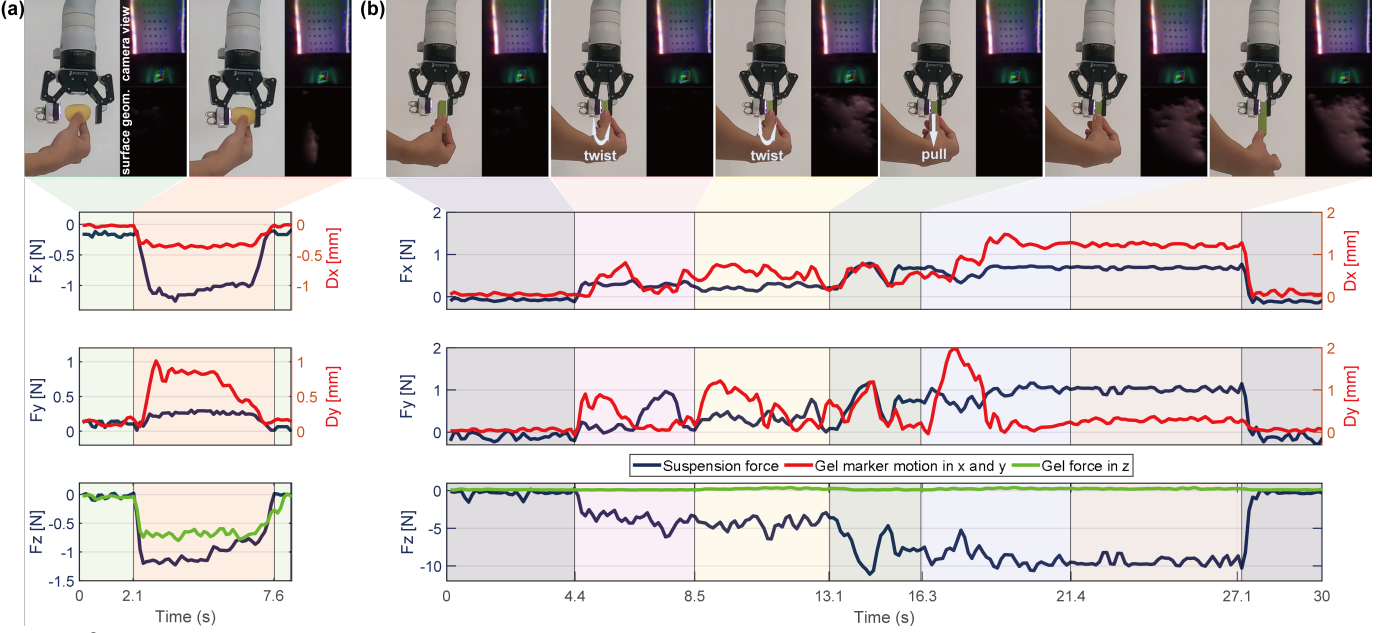


Fig. 8: **L^3 F-TOUCH sensor's contact geometry and force sensing capability.** (a) Gripping a piece of fragile potato chip. (b) Gripping a flat brick with smooth contact. The L^3 F-TOUCH produced reliable three-axis force measurement in both cases whereas the elastomer alone became insufficient. On the other hand, the elastomer augmented three-axis forces with contact geometry, producing richer tactile data than force sensors alone.

alone. The result is illustrated in Fig. 7. As can be seen that the force derived from the Gel's deformation was quickly saturated at $0.8 N$ when it reached a $1.3 mm$ deformation which was close to the thickness of the Gel ($1.5 mm$). In contrast, the suspension structure achieved a range of $10 N$ reliably, effectively overcoming the limitation of force sensing using elastomer alone or using GelSight sensors in general.

Although making the coated Gel thicker seems to be an easy and intuitive solution to extend traditional GelSight sensors' force sensing range, it would cause several complications, such as increased sensor size, shear deformation, poor illumination condition, blurry images taken from the camera, etc., which require huge engineering efforts to resolve in practice.

B. Usability in Grasping

To confirm L^3 F-TOUCH's tactile and force sensing capability in object grasping, we installed the sensor at a Robotiq 2F-85 gripper mounted to a Kinova Gen3 manipulator and conducted two grasping tasks, gripping a piece of potato chip and holding a flat brick.

Fragile object grasping: Here the robot was tasked with gripping a piece of potato chip without crashing it, see Fig. 8a. The gripper started to close at $t = 2.1 s$ and held when the Gel of elastomer deformed above $0.5 mm$, until the gripper reopened at $t = 7.6 s$. We could see that the elastomer who measured force by Gel deformation and the suspension by elastic displacement produced similar force reading in the normal direction (F_z), showing that the proposed suspension structure in L^3 F-TOUCH is as effective as typical GelSight sensors are in capturing small forces. In addition, the suspension structure provides direct measurements on the force in xy plane whereas GelSight only provides that in an indirect manner (*i.e.* by mark motions). The elastomer structure and the suspension structure of the L^3 F-TOUCH together produce

a synergy between contact geometry and reliable three-axis force measurement, resulting in richer tactile information in robot grasping.

Large flat-surface object grasping: A number of daily objects have smooth and flat surfaces for human's comfortable grasps. But GelSight and akin sensors cannot measure contact forces when gripping these objects because the Gel deforms uniformly upon contact and lacks enough surface gradient variations. Fig. 8b shows the sensor readings and some snapshots when the robot gripped a toy brick. The surface geometry reconstructed from Gel deformation did not provide much information except when the human twisted the brick hard. Thus, the normal force reading from the elastomer remained flat. The L^3 F-TOUCH sensor effectively overcame this limitation. It reliably measured the three-axis force throughout the process and sensitively detected the slip and increased gripping force when the human tried to pull away the brick, demonstrating the efficacy of the proposed L^3 F-TOUCH sensor.

C. Deployment on UAV

As shown in Fig. 9, the proposed L^3 F-TOUCH sensor was installed on a UAV platform [30] as an interaction probe to inspect a target surface. The light-weight and wireless features of the L^3 F-TOUCH sensor make it favorable for deploying to highly mobile platforms and thus attains a wider range of potential applications.

VI. CONCLUSION

This paper presented L^3 F-TOUCH sensor that enhanced the force sensing capability of classic GelSight sensors while being Light-weight, Low-cost and wireLess. The sensor's elastomer structure is similar to a GelSight that can measure

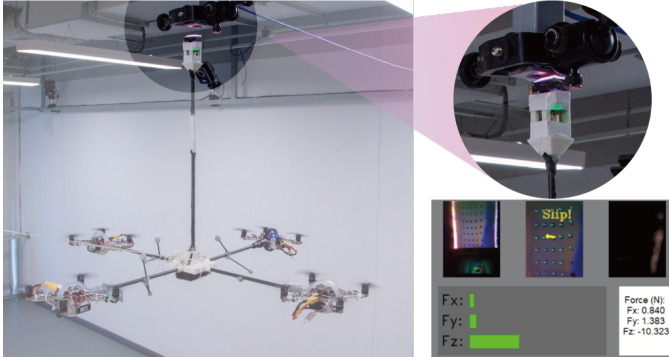


Fig. 9: Deployment of the proposed L^3 F-TOUCH sensor on a UAV to accomplish surface inspection task. The sensor's wireless and light-weight features allow dynamic mobile platforms to measure contact force and geometry in more challenging settings.

contact geometry with a super high spatial resolution. The compact suspension structure allows the elastomer to displace upon contact, which projects a marker printed on the base differently to the camera view through a mirror. A calibration method was subsequently developed to transform the marker movements to three-axis force; thus, L^3 F-TOUCH achieved a much larger range of force measurements than a GelSight does. The L^3 F-TOUCH further integrated a wireless camera module to reduce its size and deployment effort, opening up new opportunities for using VBTS.

Future work will focus on extending the sensor's capability from three-axis force to six-axis force and torque while remaining accurate and compact. The sensor's sensitivity can also be improved by adjusting the suspension structure. The wireless transmission feature can be further enhanced through improved protocol and decoding configurations. These improvements will be helpful for end-effector manipulation tasks.

Acknowledgement: We thank Dr. Boren Li, Mr. Zihang Zhao and Mr. Hang Li at BIGAI, Dr. Yohan Noh at Brunel University London for their insightful comments, and Mr. Mish Toszeghi for proofreading.

REFERENCES

- [1] M. Gentilucci, I. Toni, E. Daprati, and M. Gangitano, "Tactile input of the hand and the control of reaching to grasp movements," *Experimental brain research*, vol. 114, no. 1, pp. 130–137, 1997.
- [2] R. S. Johansson and J. R. Flanagan, "Coding and use of tactile signals from the fingertips in object manipulation tasks," *Nature Reviews Neuroscience*, vol. 10, no. 5, pp. 345–359, 2009.
- [3] W. Yuan, S. Dong, and E. H. Adelson, "Gelsight: High-resolution robot tactile sensors for estimating geometry and force," *Sensors*, vol. 17, no. 12, p. 2762, 2017.
- [4] W. Li, A. Alomainy, I. Vitanov, Y. Noh, P. Qi, and K. Althoefer, "F-touch sensor: Concurrent geometry perception and multi-axis force measurement," *IEEE Sensors Journal*, vol. 21, no. 4, pp. 4300–4309, 2020.
- [5] Y. She, S. Q. Liu, P. Yu, and E. Adelson, "Exoskeleton-covered soft finger with vision-based proprioception and tactile sensing," in *Proceedings of International Conference on Robotics and Automation (ICRA)*, 2020.
- [6] W. K. Do and M. Kennedy, "Densetact: Optical tactile sensor for dense shape reconstruction," in *Proceedings of International Conference on Robotics and Automation (ICRA)*, 2022.
- [7] S. Q. Liu and E. H. Adelson, "Gelsight fin ray: Incorporating tactile sensing into a soft compliant robotic gripper," in *International Conference on Soft Robotics (RoboSoft)*, IEEE, 2022.
- [8] "Ati multi-axis force/torque sensors family." <https://www.ati-ia.com/products/ft/sensors.aspx>.
- [9] J. A. Fishel and G. E. Loeb, "Sensing tactile microvibrations with the biotac—comparison with human sensitivity," in *International conference on biomedical robotics and biomechatronics (BioRob)*, IEEE, 2012.
- [10] J. Kim, M. Lee, H. J. Shim, R. Ghaffari, H. R. Cho, D. Son, Y. H. Jung, M. Soh, C. Choi, S. Jung, et al., "Stretchable silicon nanoribbon electronics for skin prosthesis," *Nature communications*, vol. 5, no. 1, pp. 1–11, 2014.
- [11] J. Park, M. Kim, Y. Lee, H. S. Lee, and H. Ko, "Fingertip skin-inspired microstructured ferroelectric skins discriminate static/dynamic pressure and temperature stimuli," *Science advances*, vol. 1, no. 9, p. e1500661, 2015.
- [12] Y. Yu, J. Li, S. A. Solomon, J. Min, J. Tu, W. Guo, C. Xu, Y. Song, and W. Gao, "All-printed soft human-machine interface for robotic physicochemical sensing," *Science Robotics*, vol. 7, no. 67, p. eabn0495, 2022.
- [13] W. Yuan, R. Li, M. A. Srinivasan, and E. H. Adelson, "Measurement of shear and slip with a gelsight tactile sensor," in *Proceedings of International Conference on Robotics and Automation (ICRA)*, 2015.
- [14] Y. She, S. Wang, S. Dong, N. Sunil, A. Rodriguez, and E. Adelson, "Cable manipulation with a tactile-reactive gripper," *International Journal of Robotics Research (IJRR)*, vol. 40, no. 12–14, pp. 1385–1401, 2021.
- [15] W. Yuan, Y. Mo, S. Wang, and E. H. Adelson, "Active clothing material perception using tactile sensing and deep learning," in *Proceedings of International Conference on Robotics and Automation (ICRA)*, 2018.
- [16] W. Yuan, M. A. Srinivasan, and E. H. Adelson, "Estimating object hardness with a gelsight touch sensor," in *Proceedings of International Conference on Intelligent Robots and Systems (IROS)*, 2016.
- [17] D. Ma, E. Donlon, S. Dong, and A. Rodriguez, "Dense tactile force estimation using gelslim and inverse fem," in *Proceedings of International Conference on Robotics and Automation (ICRA)*, 2019.
- [18] M. Lambeta, P.-W. Chou, S. Tian, B. Yang, B. Maloon, V. R. Most, D. Stroud, R. Santos, A. Byagowi, G. Kammerer, et al., "Digit: A novel design for a low-cost compact high-resolution tactile sensor with application to in-hand manipulation," *IEEE Robotics and Automation Letters (RA-L)*, vol. 5, no. 3, pp. 3838–3845, 2020.
- [19] S. Wang, Y. She, B. Romero, and E. Adelson, "Gelsight wedge: Measuring high-resolution 3d contact geometry with a compact robot finger," in *Proceedings of International Conference on Robotics and Automation (ICRA)*, 2021.
- [20] H. Liu, C. Zhang, Y. Zhu, C. Jiang, and S.-C. Zhu, "Mirroring without overimitation: Learning functionally equivalent manipulation actions," in *Proceedings of AAAI Conference on Artificial Intelligence (AAAI)*, 2019.
- [21] H. Tugal, K. Cetin, Y. Petillot, M. Dunnigan, and M. S. Erden, "Manipulation at optimum locations for maximum force transmission with mobile robots under environmental disturbances," *Autonomous Robots*, vol. 46, no. 6, pp. 769–782, 2022.
- [22] S. Dong, W. Yuan, and E. H. Adelson, "Improved gelsight tactile sensor for measuring geometry and slip," in *Proceedings of International Conference on Intelligent Robots and Systems (IROS)*, 2017.
- [23] A. Tandon, P. Shukla, and H. K. Patel, "Review of transduction techniques for tactile sensors and a comparative analysis of commercial sensors," in *International Conference on Multidisciplinary Research & Practice*, 2015.
- [24] B. Romero, F. Veiga, and E. Adelson, "Soft, round, high resolution tactile fingertip sensors for dexterous robotic manipulation," in *Proceedings of International Conference on Robotics and Automation (ICRA)*, 2020.
- [25] R. Ouyang and R. Howe, "Low-cost fiducial-based 6-axis force-torque sensor," in *2020 IEEE International Conference on Robotics and Automation (ICRA)*, pp. 1653–1659, IEEE, 2020.
- [26] K. Nozu and K. Shimonoura, "Robotic bolt insertion and tightening based on in-hand object localization and force sensing," in *IEEE/ASME International Conference on Advanced Intelligent Mechatronics (AIM)*, IEEE, 2018.
- [27] J. Kannala and S. S. Brandt, "A generic camera model and calibration method for conventional, wide-angle, and fish-eye lenses," *IEEE Transactions on Pattern Analysis and Machine Intelligence (TPAMI)*, vol. 28, no. 8, pp. 1335–1340, 2006.
- [28] "Aruco marker detection." https://docs.opencv.org/4.x/d9/d6a/group_aruco.html.
- [29] M. Zorrilla, Á. Martín, F. Mogollón, J. García, and I. G. Olaizola, "End to end solution for interactive on demand 3d media on home network devices," in *International Symposium on Broadband Multimedia Systems and Broadcasting*, IEEE, 2012.
- [30] Y. Su, C. Chu, M. Wang, J. Li, L. Yang, Y. Zhu, and H. Liu, "Downwash-aware control allocation for over-actuated uav platforms," in *Proceedings of International Conference on Intelligent Robots and Systems (IROS)*, 2022.